energies

MDPI

Review

Localized Heating to Improve the Thermal Efficiency of Membrane Distillation Systems

Alessandra Criscuoli * and Maria Concetta Carnevale

Institute on Membrane Technology (CNR-ITM), Via P. Bucci 17/C, 87036 Rende, CS, Italy
* Correspondence: a.criscuoli@itm.cnr.it; Tel.: +39-0984-492118

Abstract: Membrane distillation (MD) is a thermal-based membrane operation with high potential for the treatment of aqueous streams. However, its implementation is limited and only few examples of MD pilots can be found in desalination. One of the reasons behind this is that MD requires thermal energy for promoting the evaporation of water, which implies higher energy consumption with respect to pressure-driven membrane operations, like reverse osmosis (RO). Recently, among the different methods investigated to improve the thermal efficiency of MD, attempts for obtaining a localized heating of the feed, close to the membrane surface, were carried out. This work reviews experimental activities on the topic, dealing with both modified membranes, used under solar irradiation or coupled to an electric source, and specifically designed heated modules. The main results are reported and points of action for further optimization are identified. In particular, although at an early stage, this type of approach led to improvements in membrane flux and to a reduction of energy consumption with respect to conventional MD. Nevertheless, long tests to ensure a stable performance time, the optimization of operating conditions, the development of methods to control fouling issues, and the identification of the best module design, together with the scale-up of membranes/modules developed, represent the main research efforts needed for future implementation of localized heating strategy.

Keywords: electrical heating; irradiation heating; flux; energy consumption

Citation: Criscuoli, A.; Carnevale, M.C. Localized Heating to Improve the Thermal Efficiency of Membrane Distillation Systems. *Energies* **2022**, *15*, 5990. https://doi.org/10.3390/en15165990

Academic Editor: Chanwoo Park

Received: 26 July 2022
Accepted: 17 August 2022
Published: 18 August 2022

1. Introduction

Water scarcity today affects many countries worldwide. Climate change, due to the greenhouse effect, significantly increased the number of regions suffering from drought. As an example, as this article is being written, Italy is experiencing one of the driest seasons with the water flows of the most important rivers reduced by 90% in some areas. In addition to the problem of drought, population growth, as well as the intensive industrial activities contributed in recent years to the depletion of fresh water sources available on the planet. The recovery of purified water, to be re-used from polluted streams is thus becoming an urgent need. In this respect, membrane distillation is among the membrane operations most investigated because of the possibility of rejecting all non-volatile species present in the same unit into the feed, leading to a high-concentrated retentate and to a high-quality water (distilled water) as permeate [1–3]. It has been successfully applied in different fields, like ultrapure water production, purification of textile effluents, olive mill waste waters and heavy metal-contaminated waters, juice concentration, brackish and seawater desalination, and brine treatment. The basic principle is to use a hydrophobic microporous membrane for aqueous feed evaporation. In particular, one side of the membrane is in direct contact with the aqueous stream and by creating a difference of vapor pressure at the two membrane sides the liquid starts to evaporate at the feed-membrane pore mouths. Then the formed water vapor migrates through the micropores to be recovered as liquid at the permeate side. The driving force being a difference of vapor pressures rather than a difference of pressures, MD is less affected by osmotic limitations, encountered in RO therefore, higher

water recovery factors can be obtained. However, to make the liquid water evaporate there is a need to heat the feed stream. Although MD works at lower temperatures than conventional distillation columns (typical MD temperatures range from 40 to 80 °C), the thermal energy supply represents one of the main obstacles for the implementation of MD at a commercial scale. The energy consumption per produced permeate can be reduced by acting both on the productivity of the process and on the effective use of the thermal energy supplied. Given that MD is a thermal-driven operation the trans-membrane flux and thus, the productivity (defined as the amount of produced permeate) depends not only on the membrane properties but also on the thermal efficiency (e.g., temperature established at the membrane surface for water evaporation). Therefore, an improvement of thermal energy use during the operation is crucial. In MD thermal losses into the environment through the pipelines and the membrane module can occur. Furthermore, the permeate acquires the heat of condensation of the water vapor. If not recovered, this is another step where the heat supplied is lost. The thermal losses to the outside can be decreased by a proper insulation of the circuit and of the module, and choosing low-conductive materials will also assist in their realization. Concerning the heat recovery from the permeate, the use of a heat exchanger in which the feed is pre-heated while the permeate is cooled, as well as the design of modules with internal heat recovery are possible solutions [4–10]. In addition to the reduction of heat losses, the energy efficiency of MD is also based on the minimization, especially at the feed side, of the temperature polarization which consists of the temperature gradient created between the bulk of the stream and the membrane surface. For an optimal evaporation process, it is desirable to have the membrane surface at the same temperature as the bulk, so as to effectively use the warm stream. However, the membrane temperature is often lower than that of the bulk, due to the heat transfer resistance offered by the boundary layer (Figure 1), therefore, the water evaporation is lower than that achievable at the feed bulk temperature. Moreover, during the MD process, the temperature at the membrane surface further decreases because of the evaporative cooling of the water in contact with the membrane.

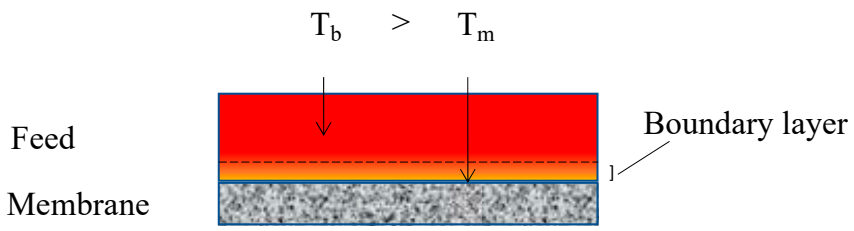

Figure 1. Temperature difference at the feed side, due to the boundary layer resistance.

An increase of the feed flow rate and/or the realization of modules with baffles/turbulence promoters could enhance the turbulence inside the module, thus reducing the boundary layer resistance [11–14]. However, pressure drops must be carefully controlled, in order to not overcome the liquid entry pressure value of the membrane with a consequent wetting of micropores. On the other hand, the temperature reduction caused by the water evaporation could not be avoided by the above strategies. Recently, the possibility of applying localized heating was investigated as a new approach to enhance the thermal performance of MD through the reduction of the temperature polarization at the feed side. In particular, both the heating inside the module and the direct heating of the membrane surface were studied. In the first case, heat was supplied to the module, without changing the membrane properties, while in the second case the membrane itself was also modified. Both approaches had the aim of increasing the temperature of the feed at the membrane surface, thus enhancing the water evaporation and the permeate production. By acting on the temperature close to the membrane surface, the cooling effect of the evaporation can also be better compensated. Solar and electrical energy sources were used to provide heat. Research in the field has significantly increased in last years and in this contribution, the

main experimental activities carried out on localized heating are presented and discussed. Future research needs are also underlined.

2. Basic Indicators in Membrane Distillation

The performance of membrane distillation can be evaluated in terms of some specific indicators (well-known and conventionally used in MD), like the water vapor transmembrane flux, which is linked to the process productivity, the temperature polarization factor, which takes into account the difference between the feed temperature in the bulk liquid and at the membrane surface, as well as the indicators linked to the energy consumption of the process and to the thermal energy use for evaporation. When solar irradiation is employed for localized heating another indicator, solar efficiency, is introduced. In the following section, definitions and main equations to be used are reported.

Permeate flux (J)

The distillate flux J is calculated using the following equation:

$$J = \frac{m}{A_{mb} \cdot \mathrm{t}} \tag{1}$$

where:

J = distillate flux ($L \cdot m^{-2}\ h^{-1}$) or ($kg \cdot m^{-2}\ h^{-1}$);
m = mass of distillate produced (kg);
A_{mb} = membrane area (m^2);
t = time (h).

High permeate fluxes are desired to ensure high productivities (high permeate production) of the system.

Temperature Polarization Factor (TPF)

The *TPF* (temperature polarization factor) is defined as:

$$TPF = \frac{T_f^m}{T_f^b} \times 100 \tag{2}$$

where:

T_f^m = membrane surface temperature at the feed side (°C);
T_f^b = bulk temperature of the feed (°C).

TPF < 1 indicates that the temperature at the membrane surface is lower than that of the feed bulk. This implies that the evaporation occurs at a lower temperature, with a consequent lower permeate flux.

Specific Energy Consumption (SEC)

SEC is defined as the amount of total energy supplied (thermal and electrical) with respect to the produced distillate ($kW \cdot kg^{-1}$). In a formula:

$$SEC = \frac{Q_T}{m} \tag{3}$$

where:

Q_T = total energy supplied (kW);
m = mass of distillate produced (kg).

Low *SEC* values are desired to work with low energy consumptions and high productivities of the system.

Gain Output Ratio (GOR)

GOR is a key performance indicator which shows the relation between the energy needed for the feed evaporation and the overall thermal energy supplied. In a formula:

$$GOR = \frac{m_d \cdot \Delta H}{QH \cdot} \quad (4)$$

where:

m_d = distillate flow rate (kg·h^{-1});
ΔH = enthalpy of vaporization (kJ·kg^{-1});
Q_H = overall thermal energy supplied (kJ·h^{-1}).

A $GOR > 1$ indicates a good use of the heat supplied. Its value depends on the membrane and module properties, on the operating conditions, and on the heat recovery systems adopted. At lab scale a $GOR < 1$ is often registered [15], while at a larger scale a value > 10 can be obtained.

Solar Efficiency

The solar efficiency of the process is defined as the ratio between the energy used for water evaporation and the overall solar irradiance. In formula [16]:

$$Solar\ Efficiency = \frac{J \cdot \Delta H}{I} \quad (5)$$

where:

J = distillate flux (kg·m^{-2}·s^{-1});
ΔH = enthalpy of vaporization (kJ·kg^{-1});
I = incident light intensity (kJ·m^{-2}·s^{-1}).

High solar efficiencies are desired to effectively use the solar irradiance supplied to the system.

3. Localized Heating with Modified Membranes

Membranes were modified in order to make themselves "heating units" inside the modules. Modifications were carried out on the membrane surface only, as well as on the whole membrane structure. Depending on the type of membranes produced, both solar and electrical energies were supplied, so as to warm up the membrane and to enhance the water evaporation (Figure 2). In the following part, the main information on the type of membranes prepared, experimental tests, and improvements obtained with respect to traditional MD are reported. The most relevant results are summarized in Tables 1 and 2.

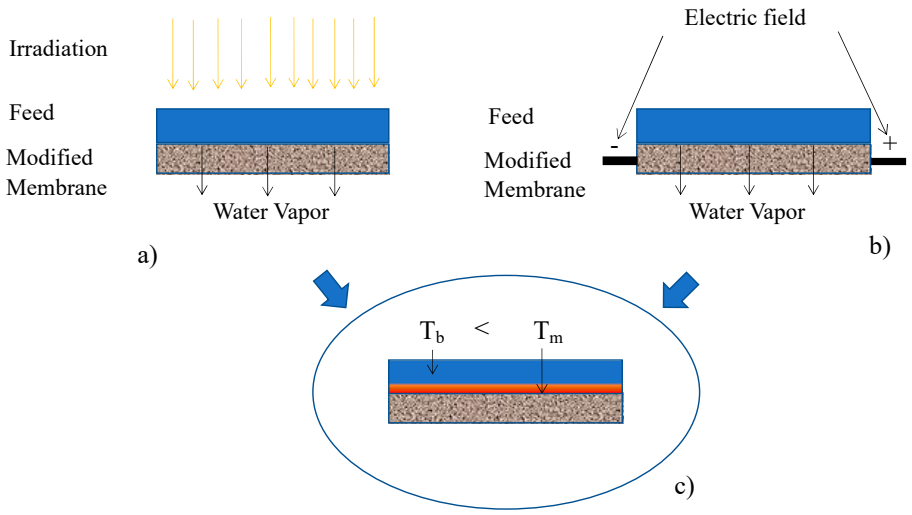

Figure 2. Modified membranes under (**a**) irradiation, (**b**) electrical field, and (**c**) temperature difference at the feed side.

3.1. Electrical Heating on Modified Membranes

Song et al. [17] employed a nichrome resistance wire (NRW) inside a polyvinylidene fluoride (PVDF) hollow fiber membrane (HFM) to realize an electro-thermal PVDF/NRW HFM module with an effective area of 20.17 cm^2. The experimental tests were carried out using a 3.5 wt% NaCl aqueous solution as feed and the vacuum membrane distillation (VMD) configuration (vacuum pressure: −0.04 MPa). The feed was heated up to 70 °C by a hot water bath. When a low direct current of 0.15 A was applied, a 2.5-fold increase of the permeate flux was measured with respect to that obtained without the application of electrical current.

A high-quality hexagonal boron nitride (hBN) nano coating was coated on stainless-steel wire cloth (SSWC), and the obtained hBN-SSWC was successively attached to a commercial PVDF membrane by Zuo et al. [18], to create a Joule heater in MD (SHMD surface heating membrane distillation). The flat SHMD module had a membrane area of 1.6 cm^2 and by starting with a 100 g/L NaCl feed a high-concentrated brine of 302.9 g/L was obtained, corresponding to a 67% single pass-recovery with a percentage of input energy utilized to produce vapor of 57%, when the energy input was 50 $kW \cdot m^{-2}$. The long-term stability of the membrane was also assessed for 100 h of operation and a spiral-wound SHMD module was produced with a percentage of input energy utilized to produce vapor of 79.1% and 875.8 $kW \cdot m^{-3}$ of energy consumption without heat recovery.

Dudchenko et al. [19] realized a stable dual-layer structure with hydrophilic–hydrophobic characteristics through the deposit of CNT (carbon nanotube)–PVA (polyvinyl alcohol) films onto a hydrophobic polytetrafluoroethylene (PTFE) membrane (area of 450 cm^2). By supplying a current, the high temperature reached at the membrane surface allowed single-pass recovery up to 100% during MD desalination tests to be registered. A GOR of 0.55 was obtained and no degradation of the CNT deposit was observed.

To cover the situations in which the solar intensity is not at the desired value (e.g., cloudy days), photothermal and Joule heating MD were coupled by using a composite membrane made of three layers: a bottom PVDF layer, a middle multi-walled carbon nanotube (MWCNT) layer, and a top polydimethylsiloxane (PDMS) layer [20]. The module's upper part had a transparent optical glass window to allow irradiation by sunlight, while the electricity was supplied through an alternating-current power source. In the bottom part, a condensation chamber was used to condense the vapor. The combined inputs of solar and electric energy allowed it to work under a constant total power. Interestingly, at the same input-power density, the Joule heating MD led to higher feed-water temperatures than the solar energy with consequent higher trans-membrane fluxes. To further optimize the performance of the Joule heating MD, Huang et al. [21] investigated different strategies. First of all, the feed was not recirculated but kept in the upper part of the cell, so as to heat just the water close to the membrane rather than the whole stream. By acting on the power supply and on the conductive layer area it was possible to further increase the temperature for the evaporation. Moreover, a three-level heat recovery design, where the condensing heat of the upper level was recovered by the feed stream of the lower level, was studied. In this case, only the first level contained the PDMS/MWCNT/PVDF membrane and underwent electrical energy supply, while the second and the third levels were only equipped with PVDF membranes. By moving from a single-level to a three-level system, the water flux increased by 2-fold with a GOR of 1.89.

Ahmed et al. [22] prepared an electrically conductive carbon nanostructure (CNS) coated polypropylene (PP) membrane and tested it in a direct contact membrane distillation (DCMD) configuration (membrane area, 22.5 cm^2) with and without applying current, while the circulating feed was externally heated. At 60 °C, the electrical current supply led to a 61% increase of flux (22.9 vs. 14.2 $kg \cdot m^{-2}\ h^{-1}$) and to a reduction of the specific energy consumption higher than 50% (1.7 vs. 3.7 $kW \cdot m^{-3}$).

In the study of Li et al. [23] a new methodology that used a composite RGO (reduced graphene oxide)-PTFE (polytetrafluoroethylene) membrane for reverse Joule heating air gap MD (AGMD) was presented. In particular, the layer of RGO Joule heating was located

at the air gap side and the contact with the feed brine, which could cause water splitting and RGO degradation in saline environments, was prevented by the PTFE membrane. A membrane module of 29.65 cm^2 was used to carry out the experiments and it was demonstrated that the permeate flux was kept stable during 115 h of testing at a value around 1 (as normalized flux), indicating that the RGO layer had good stability.

Subrahmanya et al. [24] tested a graphene-PVDF flat membrane Joule heater for VMD desalination. The graphene and PVDF content were varied from 10 to 25% and from 1 to 10%, respectively, with respect to the solvent N-Methyl-2-pyrrolidone (NMP). Desalination tests were carried out with a module of 778.54 mm^2 membrane area and best results were obtained for the graphene 2.5-PVDF1 membrane, working at the lowest feed flowrate (1 mL/min) and with an energy supply of 2 W, for which a temperature of 56 °C was registered on the membrane surface and the GOR was 5.72.

Metallic (stainless steel—SS) hollow fiber membranes were coated or impregnated with PDMS and used in sweep gas membrane distillation (SGMD) for water evaporation tests under electrical heating [25]. The membrane area at the lumen side, where dry air flowed, was 140 cm^2 and experiments were carried out at different water inlet temperatures. In all tests, by supplying electrical energy, water evaporation flux enhancement factors were registered, ranging from 1.1 to 1.4.

Anvari et al. [26] have studied a new IH (induction heating)-VMD system based on a 'self-heating' composite membrane realized by spraying a coating of iron oxide-carbon nanotubes on a hydrophobic PTFE commercial membrane. The induction heating allowed the membrane surface to heat in a contactless mode. The membrane module (32 cm^2) was made of nylon and was used for both IH-VMD and traditional VMD tests (with a commercial unmodified PTFE membrane) in the same operating conditions. For a 35 g/L NaCl feed, the IH-VMD system led to an 8-fold higher trans-membrane flux (4 vs. 0.5 $kg{\cdot}m^{-2}\ h^{-1}$) and to a 6-fold lower specific energy consumption (197 vs. 1202 $W{\cdot}kg^{-1}$). The GOR was 3.45.

3.2. Irradiation Heating on Modified Membranes

The studies of Politano et al. [27,28] illustrated a plasmonic photothermal MD process that employed asymmetric PVDF flat-sheet microporous membranes in which metallic Ag NPs (nanoparticles) were incorporated in variable percentages (from zero to 25%). The authors carried out tests using the VMD configuration with a UV lamp (with a wavelength of 366 nm) to irradiate 21.24 cm^2 of membrane area through a quartz window. The best results were obtained with a 25% Ag NPs load: for a 0.5 M feed solution at an initial temperature of 303 K, the bulk temperature was increased by about 4 K, the trans-membrane flux (25.7 $kg{\cdot}m^{-2}\ h^{-1}$) was 9-fold higher than the corresponding value for the unloaded membrane, while the temperature polarization factor (TPF) moved from 98.25% (unloaded membrane) to 106.5%, due to the interface temperature being higher than that in the bulk.

Ag photothermal nanoparticles (Ag NPs) were also incorporated in different amounts into a hydrophobic PVDF nanofibrous membrane by Ye et al. [16] to carry out tests of ultraviolet light driven DCMD. The electrospinning technique was applied and an effective membrane area of 12 cm^2 was located inside a module with a quartz window. The best performance was reached with the membrane containing 20 wt% Ag NPs, leading to the highest flux and solar efficiency (53%) during 60 h of testing.

A mixed matrix of hydrophobic photoactive membrane was prepared by Pagliero et al. [29] by dispersing carbon black (CB) in a PVDF dope solution and using NIPS (non-solvent induced phase separation) as a preparation technique. Then, VMD tests were carried out on a 30 cm^2 membrane area located in a membrane module made of PMMA (transparent polymethylmethacrylate) which was irradiated. The best performances were obtained with the membrane containing 7.5 wt% CB, with a 2-fold increase of the trans-membrane flux with respect to the pristine PVDF membrane (2.3 vs. 1 $kg{\cdot}m^{-2}\ h^{-1}$).

Dongare et al. [30] used CB NPs for the preparation of a photothermal membrane consisting of two layers: a hydrophilic polyvinyl alcohol (PVA) coating, with a thickness

of 25 μm, deposited onto a commercial PVDF membrane. Tests were carried in a DCMD configuration (countercurrent mode) sending at the feed side a 1% NaCl solution, whereas at the distillate side flowed deionized water. A quartz window (3.3 cm × 6.8 cm) allowed the irradiation of the membrane at the feed side without additional heat sources, leading to a solar efficiency of over 20%. When compared with the traditional MD, at parity of operating conditions, a higher flux was obtained at low feed velocity (0.3 vs. 0.05 kg· m^{-2} h^{-1}).

Said et al. [31] carried out tests with a membrane prepared by directly coating functionalized CB NPs on a commercial hydrophobic PTFE membrane. The membrane module had an area of 0.17 m^2 and was equipped with a transparent window of durable Plexiglas. A polycrystalline solar panel was used to supply energy and in cloudy conditions a reduction of the experimental flux was registered (0.12 kg·m^{-2} h^{-1} at 88 W·m^{-2}) with an average value of 0.55 kg·m^{-2} h^{-1}.

Wu et al. [32] used PVDF membranes coated with CB NPs or SiO_2/Au for direct solar DCMD tests on a 28.3 cm^2 membrane area, which was irradiated through a quartz window with simulated sunlight obtained using six halogen tungsten lamps. Ultrapure water was sent at the cold side and 1% NaCl solution at 35 °C was used as the feed. The sample with a CB coating density around 0.14 g m^{-2} led to the highest permeate flux with a 15% increase with respect to that achieved in tests without irradiation.

A CB NPs-coated PVDF membrane (25 cm^2) was developed and used by Tanvir et al. [33] in a passive, single-stage, permeate-side-heated solar MD unit. In this case, the feed filled a bottom chamber and was in contact with the PVDF side of the membrane while the CB coating was irradiated. The evaporated water was condensed at the top side in a condensing chamber equipped with a reflective cover. Seawater, canal water, and wastewater were treated, and initial fluxes were 1.48, 1.34, and 1.32 kg·m^{-2} h^{-1}, respectively. Corresponding operating time were 32, 18, and 10 days, after which, wetting was observed due to scaling, organic fouling, and the presence of surfactants, respectively. Interestingly, the produced permeates were of high-quality, but contained dichloromethane and methyl ethyl ketone, probably originating from the acrylic cement used for fixing the system. Under natural sunlight (652 W·m^{-2}) the energy efficiency was 67.5%.

In the work of Chen et al. [34] a PVDF membrane surface was coated by 1H,1H,2H,2H-Per-fluorodecyltriethoxysilane (FAS17) modified CB NPs, in order to combine the photothermal activity of CB NPs with omniphobic properties conferred by the presence of the fluorinated species. DCMD desalination tests were carried out on a flat membrane (31 cm^2), which was located in a module and was irradiated through a quartz window. The feed was sent to the module at 35 °C. Under irradiation, the composite membrane led to a 25% increase in flux with respect to the pristine PVDF (3.19 vs. 2.56 kg·m^{-2} h^{-1}). Moreover, when compared with traditional DCMD (without irradiation) a 55.6% increase of the input energy used to produce fresh water was registered. Tests with a model surfactant solution of sodium dodecyl sulfate (SDS) confirmed the omniphobic character of the produced membrane. The membrane was not affected by wetting in all the concentration ranges investigated (0.1–0.4 mM), while the PVDF membrane started to be wetted by the 0.2 mM SDS feed. This result is quite interesting for the treatment of wastewaters containing detergents, soaps, and surfactants, for which typical MD membranes suffer from loss of hydrophobicity.

Gong et al. [35] worked with a multilevel-roughness membrane by immobilizing a nanoparticle-assembled superstructure on a nanofibrous membrane. The particular membrane structure was obtained spraying a FTCS (fluorododecyltrichlorosilane)-CB (carbon black) suspensions at different concentration values (the optimal percentage was 2.0%) on a PVDF membrane. The DCMD configuration was used to carry out the experimental tests with natural seawater and oil-contaminated solutions as feed, and illumination was provided though a quartz window. During 48 h of testing, membrane stability and antifouling behavior were assessed, with solar efficiencies ranging from 55 to 67% for illuminations of 1 kW·m^{-2} and 10 kW·m^{-2}, respectively.

In the study of Wu et al. [36] a polydopamine (PDA)—coated PVDF membrane was employed in a solar-driven membrane distillation process. The PDA-PVDF membrane was subjected to a treatment of fluoro-silanization (FTCS-PDA-PVDF membrane), to increase its hydrophobicity, and was used in DCMD tests on a 0.5 M NaCl solution. Under 0.75 kW·m^{-2} and 7.0 kW·m^{-2} irradiation, the FTCS-PDA-PVDF membrane led to a corresponding trans-membrane flux 5-fold (0.49 vs. 0.09 kg·m^{-2} h^{-1}) and 19-fold higher (4.23 vs. 0.22 kg·m^{-2} h^{-1}) than that of the FTCS-PVDF membrane. Moreover, a solar efficiency of 45% and 41% were registered, under 0.75 kW·m^{-2} and 7.0 kW·m^{-2} irradiation, respectively.

Ghim et al. [37] developed a membrane by using the spray-coating with deposition of graphene onto a hydrophobic PTFE membrane with polymerized dopamine (PDA) and trichloro (1H,1H,2H,2Hperfluorooctyl) silane (FTCS). The FTCS-PDA/graphene/PTFE membrane was used in the first (upper) layer of a multi-layer stacked membrane module with air gaps, realized to recover the latent heat of vaporization, while the other layers were equipped with PTFE membranes. During tests, the feed (a salty solution) was stagnant (3 mm thick) to reduce heat losses. With four recovery layers and under 0.75 kW/m^2 of irradiation, a 105% solar efficiency was registered.

Huang et al. [38] used photothermal PVDF/ATO (antimony doped tin oxide) hybrid nanofiber membranes in VMD tests. The feed was sent to the module at 70 °C, using an external heater. When the membrane area of 19.63 cm^2 was irradiated at the highest ATO percentage (5%) a 3-fold increase of flux was registered with respect to that achieved without irradiation, sending a salty solution as feed (27 vs. 8 kg·m^{-2} h^{-1}).

A membrane with photothermal characteristics using TiN (titanium nitride) NPs, capable of absorbing sunlight and converting it into energy, was developed by Zhang et al. [39]. The support was a PVDF flat-sheet membrane, and the technique used to produce the membrane consisted of a facial two-step method: electrospun onto PVDF membrane of a TiN/PVA suspension and crosslinking of this PVA layer. The produced membrane had an area of 19.625 cm^2 and was tested in AGMD on salty solutions. The best results were achieved with the 10 wt% TiN NPs, with a solar efficiency of 64%, and an increase of 65.8% in flux (0.94 vs. 0.57 kg·m^{-2} h^{-1}) with respect to the PVDF membrane. Moreover, the TPC increased from 95.90% (PVDF) to 97.21% and the membrane was stable after 240 h of testing.

The performance of a Fe_3O_4/PVDF-HFP (co-hexafluoropropylene) membrane with high porosity in solar MD desalination, was studied by Li et al. [40]. The tests were carried out with a membrane area of 37.5 cm^2 under different irradiations for both the composite and the pristine PVDF membrane. At 1 kW·m^{-2} and 3 kW·m^{-2} irradiation values, the composite membrane showed a permeate flux 4 (0.97 vs. 0.26 kg·m^{-2} h^{-1}) and 6 (2.9 vs. 0.48 kg·m^{-2} h^{-1}) times higher than the PVDF-HFP one. The corresponding solar efficiencies were 53% and 59%, respectively. The prepared membrane was stable in 10 days of testing and showed interesting performance also as a pilot scale (at 3 kW·m^{-2}, a flux of about 22 kg·m^{-2} h^{-1} was registered).

Huang et al. [41] prepared a PDMS/CNT/PVDF trilayer membrane. Desalination MD tests were carried out in a two-level device (16 cm^2 membrane area) where the top level contained the trilayer membrane in contact with the feed, which was covered with glass for the irradiation. The second level was equipped with a PVDF membrane and used the heat from the permeate produced in the first level for heating the feed. Both levels had condensation chambers to condense the water vapor. A higher productivity than the pristine PVDF, linked to the photothermal activity of the trilayer membrane, was observed for tests carried out on only one level (the top one). In this case, a 2.4-fold increase in flux was measured (0.37 vs. 0.89 kg·m^{-2} h^{-1}), while the solar efficiency was 24.7% and 59% for the PVDF and the trilayer membrane, respectively.

Han et al. [42] developed, for the first time, a bio-derived membrane to be used in solar driven MD. Eggshell was the starting material from which a carbonized eggshell membrane (cESM) was produced and functionalized with carbon nanotubes (cESM-CNTs). When used under irradiation in DCMD tests on salty solutions at different concentrations, a stable trans-

membrane flux was obtained (2.52 times higher than that of the PVDF membrane −1.11 vs. 0.42 kg·m^{-2} h^{-1}) with a solar efficiency greater than 75.6% (vs 31.5% of the PVDF).

Tan et al. [43] used MXene as a coating on a PVDF membrane together with PDMS, to confer both photothermal and anti-fouling characteristics. DCMD tests in counter-current flow mode were carried out on a feed containing 200 mg/L bovine serum albumin (BSA) and 10 g/L NaCl. The membrane area was 37 cm^2 and was placed into a module made of acrylic. Tests were carried out by recirculating the feed at 65 °C. In prolonged tests (21 h), a reduction of 12% of the heat energy input per unit volume distillate and around 60% of the flux decline was registered, with respect to the uncoated membrane.

MXene was coated also onto commercial PTFE membranes by Mustakeem et al. [44] and tested as a self-heating source using only irradiation. The DCMD membrane module was in acrylic, housed 25 cm^2 of membrane area, and was tested on salty solutions at different concentrations. The best performances were obtained at the lowest feed concentration (0.36 g/L), at which a solar efficiency of 65.3% was registered. By increasing the feed salinity, both the vapor flux and the solar efficiency decreased, due to the higher salt amount on the MXene nanosheets which provoked a scattering of the incident light, with a consequent lower temperature at the membrane surface. Already at 10 g/L, the vapor flux decreased by ca. 40%, while the photothermal efficiency was around 38%.

Table 1. Electrical heating on modified membranes (best results).

Heating/Membrane Material	MD Configuration	Feed	Energy Supply	Flux (kg·m^{-2} h^{-1})	SEC (kW·kg^{-1})	Refs.
NRW/PVDF	VMD	3.5 wt% NaCl	3.15 W	14	11.86 [a]	[17]
hBN-SSWC/PVDF	DCMD	100 g/L NaCl	1–50	0.32–42.7	* calc: 3–1.17	[18]
CNT-PVA/PTFE	DCMD	100 g/L NaCl	50 W	7.5	1.25	[19]
PDMS-multiwalled CNT (MWCNT)/PVDF	Distillation with condensation chamber	3.5 wt% NaCl	0.4–1.6 W	0.24–1.1	n.a.	[20]
PDMS-multiwalled CNT (MWCNT)/PVDF	Three-level distillation with condensation chamber	3.5 wt% NaCl	1.6 W	2.77	0.36	[21]
CNS/PP	DCMD	10 g/L NaCl	50.4 W	22.9	1.7 [a]	[22]
RGO/PTFE	AGMD	35 g/L NaCl	5.5 W	1.1	n.a. [a]	[23]
Graphene/PVDF	VMD	3.5 wt% NaCl	2 W	23.44	0.11	[24]
SS-PDMS	SGMD	Water	12 W	0.11	n.a. [a]	[25]
Fe-CNT/PTFE **	VMD	35 g/L NaCl	0.781 kW·m^{-2} (2.46 W)	4	0.2	[26]

* calculated as the ratio between the Energy Supply for electrical localized heating (kW·m^{-2}) and the Flux (kg·m^{-2} h^{-1}). ** Induction heating. [a] external heated feed.

Table 2. Irradiation heating on modified membranes (best results).

Heating/Membrane Material	MD Configuration	Feed	Energy Supply ($kW \cdot m^{-2}$)	Flux ($kg \cdot m^{-2}\ h^{-1}$)	SEC * ($kW \cdot kg^{-1}$)	Refs.
Ag/PVDF	VMD	0.5 M NaCl	23	25.7	0.90 [a]	[27,28]
Ag/PVDF	DCMD	3.5 wt% NaCl	3.2	2.5	1.28	[16]
CB/PVDF	VMD	Deionized water	0.675	2.3	0.29	[29]
CB-PVA/PVDF	DCMD	1 wt% NaCl	0.7	0.3	2.3	[30]
CB/PTFE	VMD	40 g/L NaCl	0.088–1	0.12–0.77	0.73–1.30	[31]
CB or SiO_2-Au/PVDF	DCMD	1 wt% NaCl	1.37	6.12	0.22 [a]	[32]
CB/PVDF	Permeate-side-heated solar MD unit.	Seawater, canal water, wastewater	1.8	1.48, 1.34, 1.32	1.21, 1.34, 1.36	[33]
FAS17-CB/PVDF	DCMD	35 g/L NaCl	1	3.19	0.31 [a]	[34]
FTCS-CB/PVDF	DCMD	seawater	1–10	0.78–9	1.28–1.11	[35]
FTCS-PDA/PVDF	DCMD	0.5 M NaCl	0.75–7	0.49–4.23	1.53–1.65	[36]
FTCS-PDA-graphene/PTFE	AGMD	0.5 M NaCl	0.75	1.17	0.64	[37]
ATO/PVDF	VMD	3.5 wt% NaCl	n.a. (100 W power)	27	n.a. [a]	[38]
TiN-PVA/PVDF	AGMD	35 g/L NaCl	1	0.94	1.06	[39]
Fe_3O_4/PVDF-HFP	DCMD	3.5 wt% NaCl	1–3	0.97–2.9	1.03 [a]	[40]
PDMS/CNT/PVDF	Two-level distillation with condensation chamber	3.5 wt% NaCl	1	1.43	0.7	[41]
PDMS-multiwalled CNT (MWCNT)/PVDF	Distillation with condensation chamber	3.5 wt% NaCl	0.25–1	0.13–0.92	1.92–1.09	[20]
cESM-CNTs/PVDF	DCMD	2.9–35 g/L NaCl	1	1.11	0.90	[42]
MXene/PVDF	DCMD	200 mg/L BSA in 10 g/L NaCl	5.8	10	0.58 [a]	[43]
MXene/PTFE	DCMD	0.36 g/L NaCl	1	0.77	1.30	[44]

* calculated as the ratio between the Energy Supply for irradiation ($kW \cdot m^{-2}$) and the Flux ($kg \cdot m^{-2}\ h^{-1}$). [a] external heated feed.

3.3. Some Remarks

Localized heating of modified membranes was mainly investigated for the treatment of salty solutions. While fluxes and energy efficiency varied for the different studies, salt was always well rejected, leading to a purified permeate. Flat membranes were mainly developed (often starting from PVDF as pristine membrane material), and small membrane areas were often tested in lab-scale MD experiments. A direct comparison of the main results achieved is not easy, as they depend on various factors, such as the MD configuration, module design and operating conditions (energy supply, external heating of the feed, feed flow, etc.). Nevertheless, all studies confirmed the improvement of flux and the reduction of the energy consumption due to the higher temperature at the membrane surface. The electrical heating of modified membranes flux ranged from 0.11 to 42.7 $kg \cdot m^{-2}\ h^{-1}$, with SEC varying from 0.11 $kW \cdot kg^{-1}$ to 11.86 $kW \cdot kg^{-1}$ kg. For the irradiated modified membranes, flux and SEC ranging from 0.12 to 25.7 $kg \cdot m^{-2}\ h^{-1}$ and

from 0.22 to 2.3 kW·kg^{-1}, respectively, were registered. It was demonstrated that, at the same input-power density, the Joule heating MD is able to lead to higher feed-water temperatures than the solar energy, with consequent higher trans-membrane fluxes. The combination of electrical and solar heating can also be an interesting option to cover the periods with low solar radiation (e.g., cloudy periods). When comparing photothermal membranes to conductive ones, it must be noted that it is necessary to act both on the membrane preparation step and on the module design in order to allow the irradiation of the membrane surface. Thus, an extra step is present for their testing in MD applications (see Figure 3).

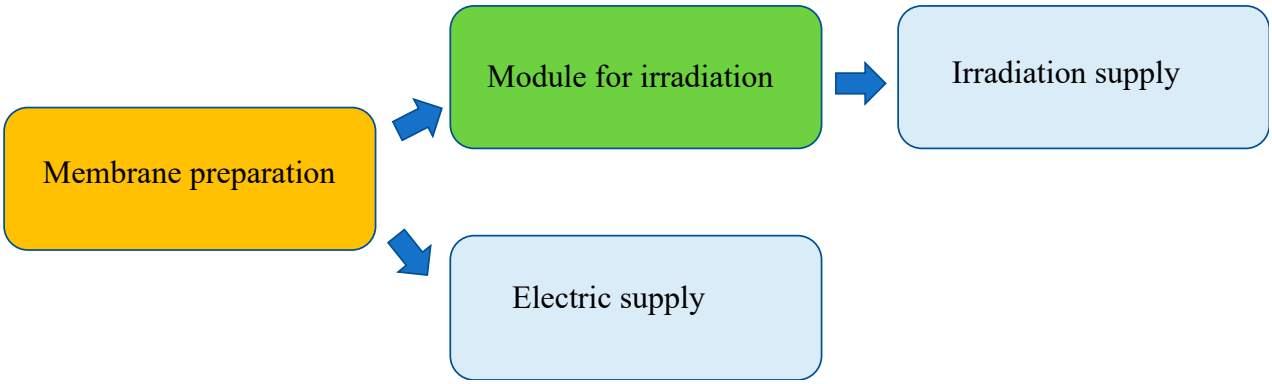

Figure 3. Main steps for localized heating on modified membranes.

4. Localized Heating Inside the Module

Different strategies were developed to heat the feed inside the module-self, through the supply of solar or electrical energy. In this case, commercial membranes were directly used without modification. In the following section, the main information on the type of module developed, experimental tests, achievements, and improvements obtained with respect to traditional MD heating (bulk feed heating) are reported. The most relevant results are summarized in Table 3, while Figure 4 depicts the investigated approaches.

Photothermal nanofluids are known to be able to absorb solar radiation and to transform solar energy into heat. A possible way to improve the solar energy use inside the module is to employ these materials in the feed of a solar powered membrane distillation (SPMD) process. This approach was investigated by Zhang et al. [45], who studied the effect of TiN (titanium nitride) NPs in AGMD tests on salty solutions. To minimize heat losses, the feed was kept static on the membrane surface (PVDF, 19.625 cm^2 membrane area) which was irradiated through a quartz window. The TiN content was varied, and the highest flux was obtained at 100 mg/L TiN. Under 1 kW·m^{-2} irradiation, a 57.4% increase of the solar energy utilization efficiency (50.5% vs. 32.1%), together with a 57% increase of flux (0.74 vs. 0.47 kg·m^{-2} h^{-1}), were registered with respect to the use of a base fluid (salty aqueous solution).

Schwantes et al. [46] proposed a configuration, named the feed gap air gap membrane distillation (FGAGMD), in which the feed was heated inside the module through a polymer film in contact with a heating stream while the permeate side worked with the traditional air gap configuration. The authors developed two plate and frame modules equipped with PTFE membranes (single module membrane area: 8 m^2) to which a salty feed (at various concentrations) was sent. With respect to the traditional spiral wound AGMD module, a 155 g/L NaCl feed in the new system led to a 9% improvement in flux (1.2 vs. 1.1 kg·m^{-2} h^{-1}), a 15-fold higher recovery ratio (45 vs. 3%), and a 9% higher thermal efficiency (50 vs. 46%), defined as the ratio between the energy needed for the feed evaporation and the overall heat transported into the module, while the GOR was lower (1.1 vs. 1.4).

A multi-stage membrane distillation (MSMD) module integrated on the backside of a commercial solar cell, so as to use the waste heat of the solar cell as heat source for MD, was realized by Wang et al. [47]. The module contained hydrophobic electrospun porous polystyrene (PS) membranes with a membrane area of 16 cm^2. Each stage consisted of a top thermal conductive layer (to transfer the heat to the liquid feed), a hydrophilic porous layer (where the evaporation occurs), a hydrophobic porous layer (through which the water vapor is transported), and a condensation layer (where the water vapor condensed). The first stage received heat from the solar panel, while in the others, the liquid water was warmed up by the latent heat of water vapor released during the condensation. With seawater as feed, by working in static conditions, the flux was slightly higher than in the configuration with feed cross-flow, due to a lower heat loss (see Table 3 for values). However, salt accumulation in the device was observed, and washing cycles were needed.

Mustakeem et al. [48] compared the traditional DCMD configuration with three types of localized heating: localized heating cross-flow (LHCF), localized heating dead-end (LHDE) with no feed circulation, and localized heating dead-end with intermittent feed channel flush (LHIF). In all cases, the membrane was in PTFE and the membrane area was 213 cm^2. The localized heating was realized locating a heating coil close to the membrane surface. In the LHCF design, the feed (Red Sea water) was re-circulated, while in the LHDE and LHIF designs, the feed filled the module by gravity. In all cases, higher flux (from 10.2 to 75%) and GOR (from 78 to 150%) and lower specific energy consumption (from 44 to 57%) than the DCMD configuration were obtained, with the LHIF design showing the best efficiency, due to the coupling of the low heat losses to the low fouling of the membrane surface. Specifically, the flux increased from 5.6 $kg{\cdot}m^{-2}\ h^{-1}$ (conventional DCMD) to 6 $kg{\cdot}m^{-2}\ h^{-1}$ (LHCF), 7.2 $kg{\cdot}m^{-2}\ h^{-1}$ (LHDE), and 9.8 $kg{\cdot}m^{-2}\ h^{-1}$ (LHIF); the GOR moved from 0.24 (conventional DCMD) to 0.6 (LHIF); the SEC decreased from 2762 $kW{\cdot}m^{-3}$ (conventional DCMD) to 1183 $kW{\cdot}m^{-3}$ (LHIF).

Table 3. Localized heating inside the modules (best results).

Heating Type	MD Configuration	Feed	Energy Supply ($kW{\cdot}m^{-2}$)	Flux ($kg{\cdot}m^{-2}\ h^{-1}$)	SEC ($kW{\cdot}kg^{-1}$)	Refs.
Photothermal nanofluid (TiN)	AGMD	35 g/L NaCl	1–5	0.74–2.77	* 1.35–1.8	[45]
Heating with a heating solution through a polymer film	FGAGMD	155 g/L NaCl	n.a.	1.2	n.a.	[46]
Solar cell-Photovoltaic panel	Three-stage MD	3.5 wt% NaCl	1	1.71 (dead-end)-1.65 (cross-flow)	* 0.58–0.61	[47]
Heating coil in the module	LHIF	Red seawater	1 kW	9.8	1.18	[48]
Aluminum layer	SHVMD-3	35 g/L NaCl	n.a.	9	1.17	[49]
Aluminum layer and aluminum meshes	VMD	100 g/L NaCl	25 W	7.6	0.87	[50]
Pt-MBT@Ag NSs/NF spacer	DCMD	0.5 M NaCl	0.8	3.6	2.5	[51]
Pt-Ni foam spacer	DCMD	5 g/L NaCl	50 W	13	2.8 ** [a]	[52]
P-G-Ni_{foam} light absorber	SVGMD	3.25–16.70 wt% NaCl Oil-contaminated water	1 1	1.13–0.96 1.07	* 0.88–1.04 * 0.93	[53]

* calculated as the ratio between the Energy Supply for localized heating ($kW{\cdot}m^{-2}$) and the Flux ($kg{\cdot}m^{-2}\ h^{-1}$). ** heater input energy per produced distillate. [a] external heated feed.

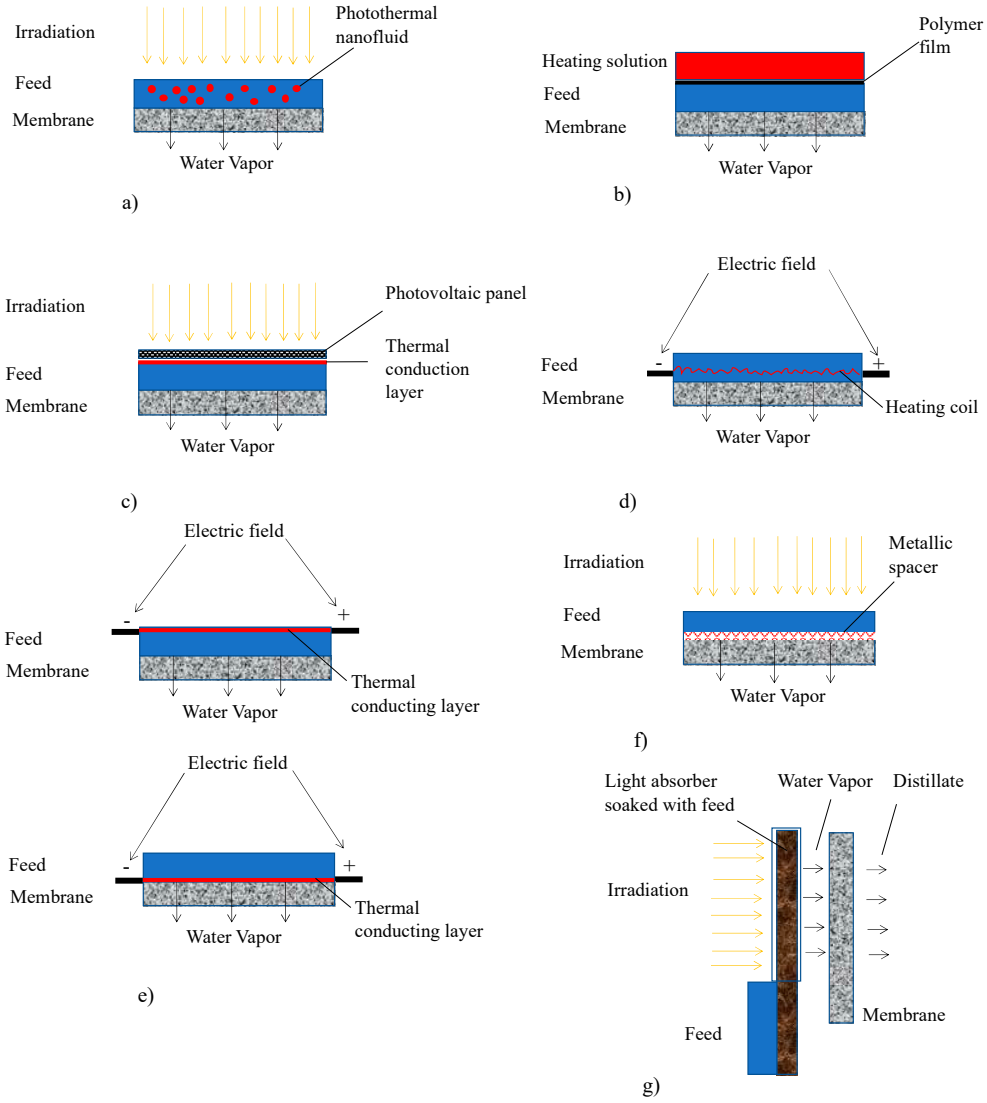

Figure 4. Investigated approaches for heating the feed inside the module through the use of (**a**) photothermal nanofluids, (**b**) a heating solution, (**c**) solar cells, (**d**) heating coils, (**e**) thermal conducting layers, (**f**) metallic spacers and (**g**) light absorbers.

Han et al. [49] used aluminum shim as thermal conducting layer in VMD desalination. Three different locations of the shim inside the cell were investigated: into the feed channel (SHVMD-1), close to the membrane surface (SHVMD-2), and both into the feed channel and close to the membrane (SHVMD-3). A hydrophobic PTFE membrane with an effective area of 40 cm^2 was used. The SHVMD-2 and SHVMD-3 designs were proven to be the most efficient ones, leading to flux values of 7 $kg \cdot m^{-2}\ h^{-1}$ and 9 $kg \cdot m^{-2}\ h^{-1}$, respectively, with corresponding SEC values of 1.1 $kW \cdot kg^{-1}$ and 1.17 $kW \cdot kg^{-1}$. A reduction of 20% in SEC at the expense of less than 10% flux reduction can be obtained through intermittent heating.

Aluminum layer and aluminum meshes were located inside a module equipped with a PP membrane (40 cm^2), to supply localized heat, by Wang et al. [50]. VMD tests were carried out on a salty feed with different direct heating configurations: aluminum layer in the feed channel, not in contact with the membrane; aluminum meshes in direct contact with the membrane (at the feed or at the distillate side); aluminum layer in the feed channel and aluminum meshes at the distillate side. The highest flux was obtained by combining the aluminum layer and meshes (7.6 $kg \cdot m^{-2}\ h^{-1}$) with an SEC of 0.87 $kW \cdot kg^{-1}$, while the lowest SEC was achieved by the mesh-only configuration (0.26 $kW \cdot kg^{-1}$) which led to a flux of 3.5 $kg \cdot m^{-2}\ h^{-1}$.

In order to overcome the issues of the membrane pore reduction and of the NPs loss under feed recirculation, which are usually encountered when modifying the membrane to heat it under solar irradiation, Ang et al. [51], created a plasmonic spacer to be used in the module. It consisted of Pt NPs grown on a porous nickel foam (NF), an Ag NP coating, and a nano-ligand (4,8-bis(methylthio)benzo [1,2-d:4,5-d0]bis [1,3]dithiole-2,6-dithione, denoted as MBT) embedded at the Pt–Ag interface (Pt-MBT@Ag NSs/NF). The spacer was located in direct contact with the membrane at the feed side and led to a 70% increase of the distillate flux with respect to the pristine NF (3.6 vs. 2.1 $kg \cdot m^{-2}\ h^{-1}$), with a photothermal efficiency of 98% under 0.8 $kW \cdot kg^{-1}$ irradiation.

Metal spacers (Ni and Cu foams) also coated with platinum nanosheets (Pt NSs) photocatalyst were employed at the feed side of a membrane module (37.1 cm^2) made of clear acrylic, so as to allow the irradiation of the feed channel, by Tan et al. [52]. Tests were carried out on a salty solution in DCMD mode with a PVDF membrane. During experiments, the feed was recirculated at 65 °C using a hot plate stirrer. All metal spacers led to similar fluxes of the traditional PP spacer. However, the heater input energy per unit volume distillate of the PP spacer was the highest (4 $kW \cdot kg^{-1}$), while with the metallic foams lower values were achieved (up to 21% lower, under irradiation, because of the absorption of the heat from the light source), and further reduced (by 28%) when the Pt-coated Ni foam spacer was used due to the photothermal conversion.

Gong et al. [53] showed a particular solar vapor gap membrane distillation (SVGMD) process where a free-standing graphene-nickel foam with polymer coating (P–G–Ni_{foam}) was prepared and used to transport (via graphene nanochannels) the feed from a sink where it was immersed. The feed was then evaporated under localized solar irradiation. The produced vapor migrated through a gap and reached a PVDF membrane, which blocked all microorganisms at one side and led to the final distillate at the other side. With this system, the direct contact of the feed and the membrane was prevented, so fouling issues were avoided. Tests were carried out on salty solutions at lab scale (membrane area 4 cm^2) and on oil/water mixture in a scaled-up system (membrane area 21 cm^2). In the second application, while the feed water was lifted to the upper part, the oil was rejected underwater, thanks to the superhydrophilic and underwater superoleophobic nature of the light absorber. A high solar efficiency (73.4% at 1 $kW \cdot m^{-2}$) was obtained during tests on salty water. When feeding oil-contaminated water, the TOC concentration in the distillate was <2 mg/L, confirming that oil was effectively rejected. Obtained fluxes are listed in Table 3.

Some Remarks

The heating of the fluid inside the module was obtained by following different strategies, with the final aim of reducing the energy needed to heat the feed (no external heating systems were used, except in one case study) and of increasing the temperature close to the membrane surface, without acting on the membrane itself. PVDF and PTFE membranes were mostly used and MD tests on salty solutions always rendered high-purity permeates. The research addressed the employment of photothermal nanofluids, heating solutions, solar cells, coils, and thermal conductive layers, as well as plasmonic spacers. A particular system where a light absorber material was used in combination with a PVDF membrane was also investigated. Typical membrane areas were in the range of 4–200 cm^2, with modules up to 8 m^2 developed when using heating solutions. As for the irradiated modified membranes, in cases where photothermal elements are used inside the module, a window for the irradiation must be designed at the feed side. When compared to conventional MD modules, better performances were achieved. Flux and SEC ranged from 0.74 $kg \cdot m^{-2}\ h^{-1}$ to 13 $kg \cdot m^{-2}\ h^{-1}$ and from 0.58 $kW \cdot kg^{-1}$ to 2.8 $kW \cdot kg^{-1}$, respectively.

5. Concluding Remarks and Future Perspectives

Localized heating was investigated as a means of improving the thermal efficiency of membrane distillation. In this respect, actions were made on the membrane properties

and on the module design. Both solar and electric energy were considered for the energy supply and, as a general result, improvements in trans-membrane flux and a reduction of energy consumptions were achieved with respect to traditional MD systems. For example, a comparison of the specific energy consumption of a localized heated MD, where a silver membrane connected with an electrical source was used, and those obtained in conventional MD configurations led to a significant difference (from 10,000–30,000 $kJ \cdot kg^{-1}$ of evaporate for localized heating versus 60,000–120,000 $kJ \cdot kg^{-1}$ for traditional DCMD and 57,600–122,400 $kJ \cdot kg^{-1}$ for conventional AGMD) [54]. Interestingly, due to heating close to the membrane surface in the investigated systems, the TPF could reach values higher than 100%, while in conventional MD it is often significantly lower. However, the higher temperature at the membrane surface could lead to the deterioration of thermolabile molecules (e.g., proteins), which, when present in the feed need to be treated. Therefore, it must be managed with care. To the best of our knowledge, no studies of localized heating for treating feeds containing thermolabile compounds were carried out until now. Nevertheless, this aspect deserves particular attention if the localized heating approach is going to be applied in the food and beverage or pharmaceutical fields. Plasmonic spacers and modified membranes, with enhanced hydrophobicity and antifouling properties, were successfully prepared and tested mainly at lab scale. The use of solar energy is certainly a sustainable choice; however, MD performance could be affected by an unstable freshwater production during periods with low solar irradiation. Membranes with good photothermal and Joule heating proved to be an interesting option to ensure a constant productivity, while reducing the electrical energy consumptions linked to the Joule heating. On the other hand, Joule heating could cause water splitting and membrane degradation in high-salinity environments, thus, isolation of the electrothermal material from saline water must be considered. It has to be noted that when modifications are carried out on membranes/spacers, an aspect of concern is the possible release in time of the heating materials used, with a consequent reduction of the system efficiency together with a pollution of the feed stream. In addition, the life time of these materials must be investigated, as well as the most appropriate strategies to reduce fouling issues without affecting the membranes/spacers properties. Commercial membranes without modification were also tested when the localized heating was made inside the module. Both localized heating strategies (acting on the membrane or acting on the module) increase the complexity of the MD plant, due to the need of specifically designed modules (especially for solar irradiation tests) and of systems for an efficient energy supply, like external electric circuits or the use of a lens to collect and concentrate solar energy. Moreover, for modules to be used under irradiation, flat membranes must be employed, with consequent reduction of the module compactness. Therefore, although encouraging results were obtained in both localized heating strategies, it is too early to make a clear choice among the tested MD units. Research is still at the first stage and further optimizations are needed in terms of type and amount of material to be used in membrane/spacer modification, power intensity, inclination of the unit to enhance solar irradiation, feed flow rate, etc. For instance, it was demonstrated that better efficiencies can be obtained without re-circulating the feed, so as to reduce the energy consumption for heating and the heat losses along the circuit. However, strategies to minimize fouling must be conceived (e.g., intermittent flushing). Moreover, lower energy consumptions were obtained with heat recovery inside the module. In addition to the above observations, for a large-scale implementation of the modified membranes and plasmonic spacers, it is also important to ensure their stability in time (long-term tests are needed) and to evaluate their ease in upscaling. Furthermore, the scaling up of the specifically designed module must also be carried out, as well as the development of systems to control the input power by artificial intelligence technologies. Therefore, there are various aspects which need further investigation before a localized heating MD can be adopted. Nevertheless, it is expected that the localized heating approach will significantly impact the application of membrane distillation in different fields.

Author Contributions: Conceptualization, A.C.; supervision, A.C.; writing—original draft preparation, A.C. and M.C.C.; writing—review and editing, A.C. All authors have read and agreed to the published version of the manuscript.

Funding: This research received no external funding.

Conflicts of Interest: The authors declare no conflict of interest.

References

1. Wang, P.; Chung, T.-S. Recent advances in membrane distillation processes: Membrane development, configuration design and application exploring. *J. Membr. Sci.* **2015**, *474*, 39–56. [CrossRef]
2. Thomas, N.; Mavukkandy, M.O.; Loutatidou, S.; Arafat, H.A. Membrane distillation research & implementation: Lessons from the past five decades. *Sep. Purif. Technol.* **2017**, *189*, 108–127. [CrossRef]
3. Deshmukh, A.; Boo, C.; Karanikola, V.; Lin, S.; Straub, A.P.; Tong, T.; Warsinger, D.M.; Elimelech, M. Membrane distillation at the water-energy nexus: Limits, opportunities, and challenges. *Energy Environ. Sci.* **2018**, *11*, 1177–1196. [CrossRef]
4. Lee, H.Y.; He, F.; Song, L.M.; Gilron, J.; Sirkar, K.K. Desalination with a cascade of cross-flow hollow fiber membrane distillation devices integrated with a heat exchanger. *AICHE J.* **2011**, *57*, 1780–1795. [CrossRef]
5. Lin, S.; Yip, N.Y.; Elimelech, M. Direct contact membrane distillation with heat recovery: Thermodynamic insights from module scale modeling. *J. Membr. Sci.* **2014**, *453*, 498–515. [CrossRef]
6. Guan, G.; Yang, X.; Wang, R.; Fane, A.G. Evaluation of heat utilization in membrane distillation desalination system integrated with heat recovery. *Desalination* **2015**, *366*, 80–93. [CrossRef]
7. Winter, D.; Koschikowski, J.; Wieghaus, M. Desalination using membrane distillation: Experimental studies on full scale spiral wound modules. *J. Membr. Sci.* **2011**, *375*, 104–112. [CrossRef]
8. Zhao, K.; Heinzl, W.; Wenzel, M.; Buttner, S.; Bollen, F.; Lange, G.; Heinzl, S.; Sarda, N. Experimental study of the memsys vacuum-multi-effect-membrane-distillation (V-MEMD) module. *Desalination* **2013**, *323*, 150–160. [CrossRef]
9. Jansen, A.E.; Assink, J.W.; Hanemaaijer, J.H.; van Medevoort, J.; van Sonsbeek, E. Development and pilot testing of full-scale membrane distillation modules for deployment of waste heat. *Desalination* **2013**, *323*, 55–65. [CrossRef]
10. Mohamed, E.S.; Boutikos, P.; Mathioulakis, E.; Belessiotis, V. Experimental evaluation of the performance and energy efficiency of a Vacuum Multi-Effect Membrane Distillation system. *Desalination* **2017**, *408*, 70–80. [CrossRef]
11. Tamburini, A.; Pitò, P.; Cipollina, A.; Micale, G.; Ciofalo, M. A thermochronic liquid crystals image analysis technique to investigate temperature polarization in spacer-filled channels for membrane distillation. *J. Membr. Sci.* **2013**, *447*, 260–273. [CrossRef]
12. Taamneh, Y.; Bataineh, K. Improving the performance of direct contact membrane distillation utilizing spacer-filled channel. *Desalination* **2017**, *408*, 25–35. [CrossRef]
13. Soukane, S.; Nacuer, M.W.; Francis, L.; Alsaadi, A.; Ghaffour, N. Effect of feed flow pattern on the distribution of permeate fluxes in desalination by direct contact membrane distillation. *Desalination* **2017**, *418*, 43–59. [CrossRef]
14. Criscuoli, A. Experimental investigation of the thermal performance of new flat membrane module designs for membrane distillation. *Int. Comm. Heat Mass Transf.* **2019**, *103*, 83–89. [CrossRef]
15. Summers, E.K.; Arafat, H.A.; Lienhard, J.H.V. Energy efficiency in comparison of single-stage membrane distillation (MD) desalination cycles in different configurations. *Desalination* **2012**, *290*, 54–66. [CrossRef]
16. Ye, H.; Li, X.; Deng, L.; Li, P.; Zhang, T.; Wang, X.; Hsiao, B.S. Silver nanoparticle-enabled photothermal nanofibrous membrane for light-driven membrane distillation. *Ind. Eng. Chem. Res.* **2019**, *58*, 3269–3281. [CrossRef]
17. Song, L.; Huang, Q.; Huang, Y.; Bi, R.; Xiao, C. An electro-thermal braid-rein- forced PVDF hollow fiber membrane for vacuum membrane distillation. *J. Membr. Sci.* **2019**, *591*, 117359. [CrossRef]
18. Zuo, K.; Wang, W.; Deshmukh, A.; Jia, S.; Guo, H.; Xin, R.; Elimelech, M.; Ajayan, P.M.; Lou, J.; Li, Q. Multifunctional nanocoated membranes for high-rate electrothermal desalination of hypersaline waters. *Nat. Nanotechnol.* **2020**, *15*, 1025–1032. [CrossRef]
19. Dudchenko, A.V.; Chen, C.; Cardenas, A.; Rolf, J.; Jassby, D. Frequency-dependent stability of CNT Joule heaters in ionizable media and desalination processes. *Nat. Nanotechnol.* **2017**, *12*, 557–563. [CrossRef]
20. Huang, J.; Tang, T.; He, Y. Coupling photothermal and Joule-heating conversion for self-heating membrane distillation enhancement. *Appl. Therm. Eng.* **2021**, *199*, 117557. [CrossRef]
21. Huang, J.; He, Y.; Shen, Z. Joule heating membrane distillation enhancement with multi-level thermal concentration and heat recovery. *Energy Convers. Manag.* **2021**, *238*, 114111. [CrossRef]
22. Ahmed, F.E.; Lalia, B.S.; Hashaikeh, R.; Hilal, N. Enhanced performance of direct contact membrane distillation via selected electrothermal heating of membrane surface. *J. Membr. Sci.* **2020**, *610*, 118224. [CrossRef]
23. Li, K.; Zhang, Y.; Wang, Z.; Liu, L.; Liu, H.; Wang, J. Electrothermally Driven Membrane Distillation for Low-Energy Consumption and Wetting Mitigation. *Environ. Sci. Technol.* **2019**, *53*, 13506–13513. [CrossRef]

24. Subrahmanya, T.M.; Lin, P.T.; Chiao, Y.-H.; Widakdo, J.; Chuang, C.-H.; Rahmadhanty, S.F.; Yoshikawa, S.; Hung, W.-S. High Performance Self-Heated Membrane Distillation System for Energy Efficient Desalination Process. *J. Mater. Chem. A* **2021**, *9*, 7868–7880. [CrossRef]
25. Shukla, S.; Méricq, J.P.; Belleville, M.P.; Hengl, N.; Benes, N.E.; Vankelecom, I.; Sanchez Marcano, J. Process intensification by coupling the Joule effect with pervaporation and sweeping gas membrane distillation. *J. Membr. Sci.* **2018**, *545*, 150–157. [CrossRef]
26. Anvari, A.; Kekre, K.M.; Azimi, Y.A.; Yao, Y.; Ronen, A. Membrane distillation of high salinity water by induction heated thermally conducting membranes. *J. Membr. Sci.* **2019**, *589*, 117253. [CrossRef]
27. Politano, A.; Argurio, P.; Di Profio, G.; Sanna, V.; Cupolillo, A.; Chakraborty, S.; Arafat, H.A.; Curcio, E. Photothermal Membrane Distillation for Seawater Desalination. *Adv. Mater.* **2017**, *29*, 1603504. [CrossRef]
28. Politano, A.; Di Profio, G.; Fontananova, E.; Sanna, V.; Cupolillo, A.; Curcio, E. Overcoming temperature polarization in membrane distillation by thermoplasmonic effects activated by Ag nanofillers in polymeric membranes. *Desalination* **2019**, *451*, 192–199. [CrossRef]
29. Pagliero, M.; Alloisio, M.; Costa, C.; Firpo, R.; Mideksa, E.A.; Comite, A. Carbon Black/Polyvinylidene Fluoride Nanocomposite Membranes for Direct Solar Distillation. *Energies* **2022**, *15*, 740. [CrossRef]
30. Dongare, P.D.; Alabastri, A.; Pedersen, S.; Zodrow, K.R.; Hogan, N.J.; Neumann, O.; Wu, J.; Wang, T.; Deshmukh, A.; Elimelech, M.; et al. Nanophotonics-enabled solar membrane distillation for off-grid water purification. *Proc. Natl. Acad. Sci. USA* **2017**, *114*, 6936–6941. [CrossRef]
31. Said, I.A.; Wang, S.; Li, Q. Field Demonstration of a Nanophotonics-Enabled Solar Membrane Distillation Reactor for Desalination. *Ind. Eng. Chem. Res.* **2019**, *58*, 18829–18835. [CrossRef]
32. Wu, J.; Zodrow, K.R.; Szemraj, P.B.; Li, Q. Photothermal nanocomposite membranes for direct solar membrane distillation. *J. Mater. Chem. A* **2017**, *5*, 23712–23719. [CrossRef]
33. Tanvir, R.U.; Sujon, S.A.; Yi, P. Passive Permeate-Side -Heated Solar Thermal Membrane Distillation: Extracting Potable Water from Seawater, Surface Water, and Municipal Wastewater at High Single-Stage Solar Efficiencies. *ACS EST Engg.* **2021**, *1*, 770–779. [CrossRef]
34. Chen, Y.R.; Xin, R.; Huang, X.; Zuo, K.; Tung, K.L.; Li, Q. Wetting-resistant photothermal nanocomposite membranes for direct solar membrane distillation. *J. Membr. Sci.* **2021**, *620*, 118913. [CrossRef]
35. Gong, B.; Yang, H.; Wu, S.; Yan, J.; Cen, K.; Bo, Z.; Ostrikov, K.K. Superstructure-Enabled anti-fouling membrane for efficient photothermal distillation. *ACS Sustain. Chem. Eng.* **2019**, *7*, 20151–20158. [CrossRef]
36. Wu, X.; Jiang, Q.; Ghim, D.; Singamaneni, S.; Jun, Y.-S. Localized heating with a photothermal polydopamine coating facilitates a novel membrane distillation process. *J. Mater. Chem. A* **2018**, *6*, 18799–18807. [CrossRef]
37. Ghim, D.; Wu, X.; Suazo, M.; Jun, Y.S. Achieving Maximum Recovery of Latent Heat in Photothermally Driven Multi-Layer Stacked Membrane Distillation. *Nano Energy.* **2021**, *80*, 105444. [CrossRef]
38. Huang, Q.; Gao, S.; Huang, Y.; Zhang, M.; Xiao, C. Study on photothermal PVDF/ATO nanofiber membrane and its membrane distillation performance. *J. Membr. Sci.* **2019**, *582*, 203–210. [CrossRef]
39. Zhang, Y.; Li, K.; Liu, L.; Wang, K.; Xiang, J.; Hou, D.; Wang, J. Titanium nitride nanoparticle embedded membrane for photothermal membrane distillation. *Chemosphere* **2020**, *256*, 127053. [CrossRef]
40. Li, W.; Chen, Y.; Yao, L.; Ren, X.; Li, Y.; Deng, L. Fe_3O_4/PVDFHFP Photothermal Membrane with in-Situ Heating for Sustainable, Stable and Efficient Pilot-Scale Solar-Driven Membrane Distillation. *Desalination* **2020**, *478*, 114288. [CrossRef]
41. Huang, J.; Hu, Y.; Bai, Y.; He, Y.; Zhu, J. Novel solar membrane distillation enabled by a PDMS/CNT/PVDF membrane with localized heating. *Desalination* **2020**, *489*, 114529. [CrossRef]
42. Han, X.; Wang, W.; Zuo, K.; Chen, L.; Yuan, L.; Liang, J.; Li, Q.; Ajayan, P.M.; Zhao, Y.; Lou, J. Bio-derived ultrathin membrane for solar driven water purification. *Nano Energy* **2019**, *60*, 567–575. [CrossRef]
43. Tan, Y.Z.; Wang, H.; Han, L.; Tanis-Kanbur, M.B.; Pranav, M.V.; Chew, J.W. Photothermal-enhanced and fouling-resistant membrane for solar-assisted membrane distillation. *J. Membr. Sci.* **2018**, *565*, 254–265. [CrossRef]
44. Mustakeem, M.; El-Demellawi, J.K.; Obaid, M.; Fangwang, M.; Alshareef, H.N. MXene-Coated Membranes for Autonomous Solar-Driven Desalination. *ACS Appl. Mater.* **2022**, *14*, 5265–5274. [CrossRef] [PubMed]
45. Zhang, Y.; Liu, L.; Li, K.; Hou, D.; Wang, J. Enhancement of Energy Utilization Using Nanofluid in Solar Powered Membrane Distillation. *Chemosphere* **2018**, *212*, 554–562. [CrossRef] [PubMed]
46. Schwantes, R.; Seger, J.; Bauer, L.; Winter, D.; Hogen, T.; Koschikowski, J.; Geißen, S.U. Characterization and Assessment of a Novel Plate and Frame MD Module for Single Pass Wastewater Concentration–FEED Gap Air Gap Membrane Distillation. *Membranes* **2019**, *9*, 118. [CrossRef]
47. Wang, W.; Shi, Y.; Zhang, C.; Hong, S.; Shi, L.; Chang, J.; Li, R.; Jin, Y.; Ong, C.; Zhuo, S.; et al. Simultaneous production of fresh water and electricity via multistage solar photovoltaic membrane distillation. *Nat. Commun.* **2019**, *10*, 3012. [CrossRef]
48. Mustakeem, M.; Qamar, A.; Alpatova, A.; Ghaffour, N. Dead-end membrane distillation with localized interfacial heating for sustainable and energy-efficient desalination. *Water Res.* **2021**, *189*, 116584. [CrossRef]

49. Han, F.; Liu, S.; Wang, K.; Zhang, X. Enhanced Performance of Membrane Distillation Using Surface Heating Process. *Membranes* **2021**, *11*, 866. [CrossRef]
50. Wang, J.; Liu, Y.; Rao, U.; Dudley, M.; Ebrahimi, N.D.; Lou, J.; Han, F.; Hoek, E.M.V.; Tilton, N.; Cath, T.Y.; et al. Conducting thermal energy to the membrane/water interface for the enhanced desalination of hypersaline brines using membrane distillation. *J. Membr. Sci.* **2021**, *626*, 119188. [CrossRef]
51. Ang, E.H.; Tan, Y.Z.; Chew, J.W. A three-dimensional plasmonic spacer enables highly efficient solar-enhanced membrane distillation of seawater. *J. Mater. Chem. A* **2019**, *7*, 10206. [CrossRef]
52. Tan, Y.Z.; Ang, E.H.; Chew, J.W. Metallic spacers to enhance membrane distillation. *J. Membrane Sci.* **2019**, *572*, 171–183. [CrossRef]
53. Gong, B.; Yang, H.; Wu, S.; Xiong, G.; Yan, J.; Cen, K.; Bo, Z.; Ostrikov, K. Graphene Array-Based Anti-fouling Solar Vapour Gap Membrane Distillation with High Energy Efficiency. *Nano-Micro Lett.* **2019**, *11*, 51. [CrossRef] [PubMed]
54. Alsaati, A.; Marconnet, A.M. Energy efficient membrane distillation through localized heating. *Desalination* **2018**, *442*, 99–107. [CrossRef]